

## Highlights

### **A vibration signal model of planetary gearboxes with unequal load sharing among planets**

Haoqun Ma,Zhipeng Feng

- Vibration signal model of unequal load sharing among planets
- Influence of gear meshing vibration, transfer path effect and natural vibration
- Analytical expression of Fourier spectrum
- Influence of planet number, error severity and input torque on spectral configuration

# A vibration signal model of planetary gearboxes with unequal load sharing among planets

Haoqun Ma<sup>a</sup>, Zhipeng Feng<sup>a,\*</sup>

<sup>a</sup>University of Science and Technology Beijing, No.30, Xueyuan Road, Haidian District, Beijing.

## ARTICLE INFO

### Keywords:

Unequal load sharing  
Planetary gearbox  
Signal model  
Fault diagnosis

## ABSTRACT

Planetary gearboxes feature large transmission ratios within compact volumes because they can share the input torque load by parallel paths formed by planets. Uneven load sharing among planets leads to inefficiency and accelerating fatigue. This paper establishes a vibration signal model to describe the association between the uneven distribution of planet loads and the vibration signal components. In the cases of low torques or severe errors, some planets will lose connection, leading to the shift of system natural frequency. The derived Fourier spectrum illustrates the spectral structure and the influences of different planet numbers, input torques, and manufacturing error severity. Numerical simulation and experimental substations agree well with the proposed theoretical model.

## 1. Introduction

Planetary gearboxes have several planets forming parallel transmission paths to split the input torque. This configuration reduces the load applied to each meshing gear and allow the planetary gearboxes to be compact. Because of the co-axial structure of planetary gearboxes, radial forces acting on the gears can be neutralized. And flexibly supported sun gears and carrier can move radially within a certain range to compensate for the manufacturing errors partially. These above mentioned merits of planetary gearboxes will compromise if the loads are unevenly applied to planets, usually arisen from manufacturing errors, such as a planet pinhole deviating from its nominal position. Unequal load sharing can also lead to efficiency loss or accelerating aging.

Most of works on the fault diagnosis of planetary gearboxes mainly concern gears [1] or bearings [2], and do not involve the planet load sharing, though the planet load sharing also significantly impacts the vibration signals.

Many investigations focus on the calculation of load sharing factors and the physical mechanism. Some conclusions contributed by previous publications are summarized as follows [3]:

- The floating (piloting) sun gear can improve the conditions of planet equal load sharing [4].
- Load sharing characteristics are primarily affected by the tangential errors, and insensitive to radial errors [5].
- Three planet gearboxes with at least one floating central members (sun gear, ring gear and carrier) can evenly distribute the load if the manufacturing errors associated with planet sharing are within a certain range [3].
- The diagonal planets in four-planet gearboxes have the same load sharing [6].
- Planet load sharing is a quasi-static problem and does not need to consider dynamic effects [7].
- Increasing the input torque can alleviate the planet load inequality [6].
- Increasing the planet number without tightening manufacturing error tolerance will deteriorate the load sharing condition [8].

Vibration signal modelling can bridge between the physical mechanism of the system and the mathematical expression both in time domain and frequency domain, facilitating the further fault diagnosis of unequal load sharing and other components. McFadden and Smith [9] probably firstly proposed that the asymmetry sidebands around the

\*Corresponding author

 fengzp@ustb.edu.cn (Z. Feng)

ORCID(s): 0000-0002-3403-4386 (Z. Feng)

## Nomenclature

|  |  |                 |   |
|--|--|-----------------|---|
| $\mathcal{F}\{\cdot\}$                               | Fourier transform  | $A_{si}$        | impulsive amplitude of $i$ -th planet-sun gear meshing                          |
| $\beta > 0$  | structural damping coefficient   | $e_i$           | tangential error of $i$ -th planet center                                       |
| $\delta(t)$  | Dirac impulse  | $F$             | strength factor of transfer path effect, proportional to the input torque $T_s$ |
| $e_i$  | angular position error of $i$ -th planet center                                    | $f_n$           | natural frequency   |
| $\text{III}(t)$                                      | Dirac comb function  | $l$             | length of a transfer path   |
| $\sigma_{ri}, \sigma_i$                              | transfer path effect on planet-ring gear   | $M$             | planet number   |
| $\sigma_{si}$  | transfer path effect on planet-sun gear  | $Z_{\{\cdot\}}$ | gear tooth number   |
| $\Theta_i$   | nominal angular position of $i$ -th planet   | $f_c$           | carrier rotation frequency  |
| $\varphi_i$  | phase difference between planet-ring and planet-sun meshing for the $i$ -th planet | $f_m$           | gear meshing frequency  |
| $\xi_{ri}, \xi_{si}$                                 | vibration originating from the $i$ -th planet-ring and planet-sun gears            | $J$             | inertia moment  |
| $\{\cdot\}_r, \{\cdot\}_p, \{\cdot\}_s, \{\cdot\}_c$ | ring gear, planet, sun gears and carrier, respectively                             | $k_e$           | effective support stiffness concerning both the bearing and gear meshing        |
| $a$  | attenuation factor of transfer path effect   | $L_i$           | load sharing ratio of the $i$ -th planet  |
| $A_{ri}$   | impulsive amplitude of $i$ -th planet-ring gear meshing                            | $R_{\{\cdot\}}$ | gear pitch circle radius  |
|  |  | $T_s$           | total torque applied on input sun gear  |

meshing frequency is ascribed to the planet revolving motion relative to the fixed transducer mounted on the ring gear. The established model of vibration signal indicates the planet number multiples of carrier order in spectrum are arisen from the planet motion. This feature originates from the signal acquisition method but not the inherent vibrational nature of planetary gearboxes. Inalpolat and Kahraman [10] took planet phases into account and categorized planetary gearboxes into five classes according to their planet angular positions (equally spaced or unequally spaced) and phases conditions (in phase, sequentially spaced phases, arbitrary phases). Mark and Hines [11] derived the Fourier-series of fixed transducer response mounted on the ring gear and explicitly explained the unequal load sharing will lead to the harmonics at non planet number multiples of tooth meshing. Lei [12] et al. proposed a phenomenological model containing the meshing vibration between the sun gear and planets as well as the effects of gear faults, further verifying the conclusions in Mark's paper.

The vibration signal model proposed in this paper based on and extends these models in the above references. We can find that natural vibration excited by the gear meshing cannot be omitted, because it globally shapes the signal envelope in frequency domain. In addition, the assumption that all planets are engaging with sun or ring gear is invalid in cases where the manufacturing errors are severe or the input torques are relatively low, especially for planet number is more than four. When some planets lose connection with sun or ring gears, the natural frequency will also shifts due to the decreased system stiffness. The derived Fourier spectrum with these considerations can better agree with the practical circumstances. As the planet number, error severity and input torque vary, the signal model and its corresponding spectra evolves. All these factors will be discussed in this paper.

Section 2 introduces the vibration signal model. The Fourier spectrum is derived in Section 3. Section 4 discusses the influence of main factors in the signal model. Experimental verification is presented in Section 5. At last, the final Section 6 concludes the above investigation.

## 2. Signal model

### 2.1. General signal model

A typical layout of planetary gearboxes consists of three kinds of gears mounted so that the centers of planet revolve around the center of sun and ring gears. This paper merely discusses the common cases of speed reducers where the

sun gear connects with the power input shaft and the carrier works as the power output, while vibration sensors are usually mounted on the surface of the stationary ring gear in diagnostic applications.

The vibration in planetary gearboxes mainly originates from the meshing of gears [13]. When the planet gears engage with the ring gear or sun gear, the number of the involved tooth varies with the relative rotation between gears and their contact stiffness changes consequently. The transmission load nominally remains constant and the gearbox is a parametrically excited multi-degree-freedom system [14].

The signal model perceived by the stationary transducer on the gearbox housing can be modelled as the summation of all planet vibration considering transfer path effect. The impulsive intensity of gear meshing is assumed to be proportional to the load applied on each planet. The vibration of each planet contains planet-ring and planet-sun parts. Thus, the general signal model is

$$x(t) = \sum_{i=1}^M L_i \cdot [\sigma_{ri}(t)\xi_{ri}(t) + \sigma_{si}(t)\xi_{si}(t)], \quad (1)$$

where  $M$  is the planet number,  $L_i$  denotes the load sharing factor,  $\sigma_{ri}$  and  $\sigma_{si}$  denotes the transfer path effect on planet-ring and planet-sun gears, respectively,  $\xi_{ri}$  and  $\xi_{si}$  are the vibration originating from the  $i$ -th planet-ring and planet-sun gears.

Nominally, all planet centers distribute along circumference of the carrier evenly. Without loss of generality, the nominal angular position of first planet center is set as zero, and

$$\Theta_i = \frac{(i-1) \cdot 2\pi}{M}, \quad (2)$$

where  $\Theta_i$  denotes the nominal angular position of  $i$ -th planet. In addition, due to the manufacturing or assembling process, each planet center deviates along the tangential direction from the nominal position by  $\epsilon_i$ . If  $\epsilon_i > 0$ , the planet engages with the ring or sun gear in advance, or negative error represents the engagement lag. We can assume  $\epsilon_1 = 0$  in the coordinate system, because these planets locate relatively to each other. Even if  $\epsilon_1 \neq 0$ , we can also set  $\epsilon_i = \epsilon'_i - \epsilon'_1, i \geq 2$ , where  $\epsilon'_i$  is  $i$ -th planet error in the new coordinate system.

To reveal the spectral structure simply, the gear meshing vibration of each planet is regarded as Dirac comb function  $\text{III}(t) = \sum_{i=-\infty}^{+\infty} \delta(t-i)$ , where  $\delta(t)$  is a single impulse. The meshing frequency can be calculated by different engaging gears,

$$f_m = Z_r \cdot (f_r + f_c) = Z_p \cdot (f_p - f_c) = Z_s \cdot (f_s - f_c). \quad (3)$$

where  $\{\cdot\}_r, \{\cdot\}_p, \{\cdot\}_s, \{\cdot\}_c$  denote ring gear, planet, sun gears and carrier, respectively,  $Z_{\{\cdot\}}$  is the gear tooth number and  $f_{\{\cdot\}}$  is the rotating frequency.

For planet-ring gears, the planet angular position error brings about the time shift. The time shift is the angular error divided by the relatively rotating velocity. Thus, the planet-ring meshing vibration can be written as

$$\xi_{ri}(t) = A_{ri} \text{III} \left[ f_m \cdot \left( t - \frac{\epsilon_i + \Theta_i}{2\pi f_c} \right) \right], \quad (4)$$

where  $A_{ri}$  is the impulsive amplitude of  $i$ -th planet-ring gear meshing,  $f_m$  is the meshing frequency. Park et al. propose the difference between planet-ring and planet-sun meshing phase [15]. Similarly, the planet-sun meshing vibration is

$$\xi_{si}(t) = A_{si} \text{III} \left[ f_m \cdot \left( t + \frac{\epsilon_i + \Theta_i}{2\pi f_s - 2\pi f_c} \right) + \frac{\varphi_i}{2\pi} \right], \quad (5)$$

where  $A_{si}$  is the impulsive amplitude of  $i$ -th planet-sun gear meshing,  $\varphi_i$  is the phase difference between planet-ring and planet-sun meshing for the  $i$ -th planet.

## 2.2. Algorithm of load sharing factors

Ligata et al. proposed an algorithm to calculate the load sharing factor through analogizing the in-plane torque balance problem to the 3-D force and momentum balance problem [16], as demonstrated in Fig. 1.

### Unequal planet load sharing

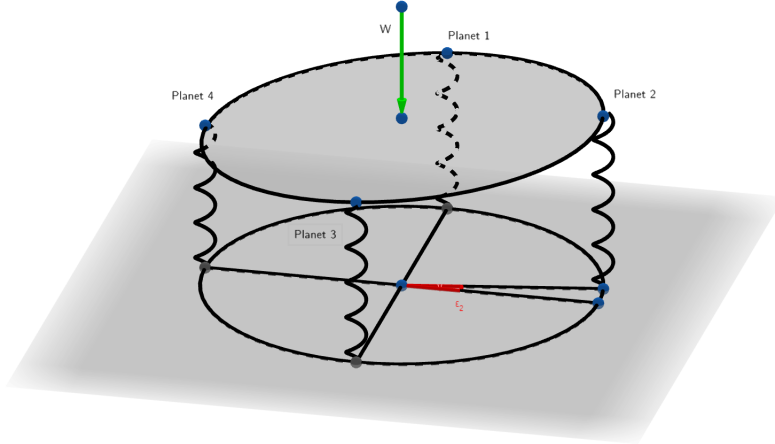


**Figure 1:** Analogical model of 4 planet load sharing: springs are analogized to planets:  $W$  is the equivalent input torque;  $\epsilon_2$  is the angular position error of second planet.

1. Initialization of parameters. Analogize the torque balance model with the planet center circle to the force and moment balance model in the axial direction perpendicular to the planet center plane. Analogize the planet gears to springs with the same stiffness  $1/k_e = 1/(k_{rp} + k_{sp}) + 1/k_b$ , where  $k_{rp} = 2.57 \times 10^8$  and  $k_{sp} = 1.67 \times 10^8$  are the meshing stiffness of planet-ring and planet-sun, respectively,  $k_b = 3.2 \times 10^7$  is the planet bearing stiffness. The tangential errors (illustrated in Fig. 2) is equivalent to the length of spring in the axial direction  $z_i = e_i = 2(R_r - R_p) \sin(\epsilon_i/2) \cos(\epsilon_i/2)$ , where  $R_p$  is the planet radius,  $R_s$  is the sun gear radius,  $\epsilon_i$  is the angular position error the  $i$ -th planet. The locations of springs accord with planet pinhole positions in the planet center plane,  $x_i = -(R_p + R_s) \sin(\Theta_i + \epsilon_i)$ ,  $y_i = (R_p + R_s) \cos(\Theta_i + \epsilon_i)$ . The input torque equals the axial load on a plate pushing on the springs,  $W = 2T_s/R_s$ . The rocking motions  $\phi_x$  and  $\phi_y$  of the plate are analogous to the floating motions of the central member in the  $x$  and  $y$  directions. The radius of the circle where planet centers locate at is  $R_b = R_s + R_p$ .

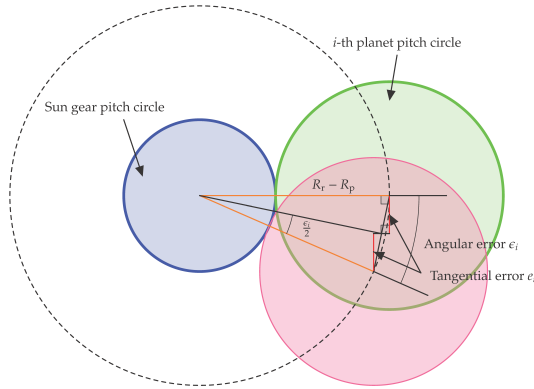


**Figure 2:** Tangential error calculation.

2. Determine the initial location of *planet center plate*. The first contacting point  $J = \arg \max_i(z_i)$ . Define a line tangent to the circle in plane  $P_1$  (parallel with the  $x$ - $y$  plane) and another point  $Q$  also on the line  $y_Q =$

$-(x_Q - x_J)x_J/y_J + y_J$ . Define the plane  $P_2$  by three points  $J, Q, K$ :

$$\begin{aligned} ax + by + cz + d &= 0, \\ a &= (y_Q - y_J)(z_K - z_J) - (y_K - y_J)(z_Q - z_J), \\ b &= (x_K - x_J)(z_Q - z_J) - (x_Q - x_J)(z_K - z_J), \\ c &= (y_K - y_J)(x_Q - x_J) - (y_Q - y_J)(x_K - x_J), \\ d &= x_Q(y_Jz_K - z_Jy_K) + x_J(y_Kz_Q - z_Ky_Q) + x_K(z_Jy_Q - y_Jz_Q). \end{aligned} \quad (6)$$

3. Transverse all  $K \neq J$  to find the second point  $K$  satisfying  $K = \arg \max_{K \neq J} \left\{ \arccos \left[ \frac{|c|}{\sqrt{a^2+b^2+c^2}} \right] \right\}$ . Define the plane  $P_3$  by the three points  $J, K, N$ . Recalculate the corresponding  $a, b, c$  for plane  $P_3$ . The third point  $N = \arg \max_{N \neq J, K} \left\{ \arccos \left[ \frac{|c|}{\sqrt{a^2+b^2+c^2}} \right] \right\}$ .
4. Verify whether the load application point  $C$  (origin point) is within the triangle  $J, K, N$  via crossing between the vectors formed by three sides, otherwise repeat the step 4.
5. Calculate the supporting forces of three points  $(J, K, N)$  by applying the force and momentum balance equations.

$$\begin{aligned} \sum F_i &= W, \\ M_x &= \sum F_i \cdot y_i = 0, \\ M_y &= \sum F_i \cdot x_i = 0, \end{aligned} \quad (7)$$

6. Consider the cases of more than three supporting planets. Obtain the  $i$ -th spring deflection  $\delta_i = \frac{F_i}{k_e}$ . Update the coordinates on the new plane  $P_d$ :  $z_i^d = z_i - \delta_i$ , as well as the  $a, b, c, d$ . Recalculate the coordinates of other points.
7. For  $H \neq J, K, N$ , if the origin length protrude the plane  $P_d$ :  $z_H > z_H^d$ , chose  $G_1, G_2$  from  $J, K, N$  to satisfy load application point  $C$  is within triangel  $HG_1G_2$ , the other residual point is denoted by  $B$ . Add the following equation to the Eq. 7.

$$F_{G_1}A_1 + F_{G_2}A_2 + F_B A_3 F_H A_4 = k_e Y. \quad (8)$$

where

$$\begin{aligned} Y &= [A_1, A_2, A_3, A_4] \cdot [z_{G_1}; z_{G_2}; z_B; z_H], \\ \eta &= \frac{(x_{G_2} - x_{G_1})(y_B - y_{G_1}) - (x_B - x_{G_1})(y_{G_2} - y_{G_1})}{(x_{G_2} - x_{G_1})(y_H - y_{G_1}) - (x_H - x_{G_1})(y_{G_2} - y_{G_1})}, \\ A_1 &= (\eta - 1)y_{G_2} + y_B - \eta y_H, \quad A_2 = (1 - \eta)y_{G_1} - y_B + \eta y_H, \\ A_3 &= y_{G_2} - y_{G_1}, \quad A_4 = \eta(y_{G_2} - y_{G_1}). \end{aligned} \quad (9)$$

8. Repeat the step 7 for all springs in contact with the plate after the load  $W$  is applied. Generally if the contacting planets are more than 3,  $N_C > 3$ , add  $N_C - 3$  equations:

$$F_{G_{1m}}A_{1m} + F_{G_{2m}}A_{2m} + F_{Bm}A_{3m} - F_{Hm}A_{4m} = K_e Y_m, \quad m \in [1, N_C - 3]. \quad (10)$$

9. Finally, the load sharing factors are  $L_i = F_i/W$ .

Unequal load sharing will gives rise to non-uniform impulsive intensity. The acceleration are linearly affected by the dynamic force exerted. Thus, the vibration amplitude of each planet is assumed to be proportional to the load applied on it [10]. In other words, planet loads modify the amplitude of the vibration signal. Moreover, the unevenly planet distribution along the angular position of carrier also has phase modulation when the transfer path is considered simultaneously. These effects will be illustrated explicitly in the later Section 4.

### 2.3. Transfer paths

The vibration originating from the planet meshing with ring or sun gear propagates through several paths to the stationary sensor mounted on the case. As demonstrated in Fig. 3, there are three paths for planet-ring and three paths planet-sun gear meshing. These transfer paths can be categorized into two types, depending on whether or not they pass through bearings. The paths passing through bearings (path 2, 3, 5, 6 in Fig. 3) must transfer via the gearbox housing to reach the sensor fixed on the top. Compared with the paths merely passing through gears (path 1, 4 in Fig. 3), these paths passing bearings are longer and more likely to be attenuated by the lubricating oil layer in bearings [1]. To simplify modelling, only the shorter paths (path 1, 4 in Fig. 3) are concerned in this paper.

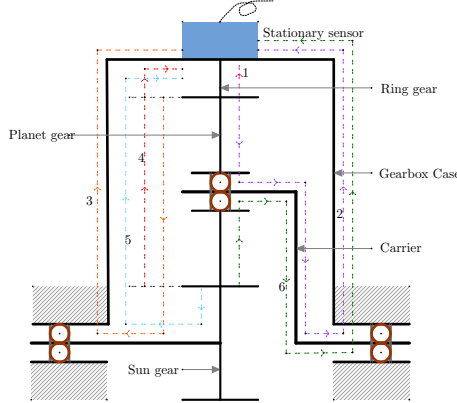


**Figure 3:** Transfer paths of gear meshing vibration: 1. planet-ring meshing point → ring gear → transducer; 2. planet-ring meshing point → planet → planet bearing → carrier → carrier bearing → gearbox case → transducer; 3. planet-ring meshing point → planet → planet-sun meshing point → sun gear shaft → sun gear bearing → gearbox case → transducer; 4. planet-sun meshing point → planet → planet-ring meshing point → ring gear → transducer; 5. planet-sun meshing point → sun gear shaft → sun gear bearing → gearbox case → transducer; 6. planet-sun meshing point → planet → planet bearing → carrier → carrier bearing → gearbox case → transducer.

The lengths of path 1 and path 4 vary with the circumferential position of carrier. For each planet, the meshing vibration points get close to the fixed sensor as the planet approaches the top surface of gearbox case. When the planet reaches the climax of its revolution circle, the fixed transducer perceives the maximum impulsive strength. While the planet arrives at the case bottom, the perceived impulses are most weakened. The path 1 length is triangle wave of time (as shown in Fig. 4(a)) when planetary gearboxes operate at a constant speed and planet distributes evenly,

$$l_{ri}(t) = \begin{cases} 2\pi R_f f_c \left| t - \left( \frac{\epsilon_i + \Theta_i}{2\pi f_c} + \frac{n}{f_c} \right) \right|, & \frac{n}{f_c} - \frac{1}{2Mf_c} + \frac{\epsilon_i + \Theta_i}{2\pi f_c} \leq t < \frac{n}{f_c} + \frac{1}{2Mf_c} + \frac{\epsilon_i + \Theta_i}{2\pi f_c}, n \in \mathbb{Z}, i = 1, 2, \dots, M \\ +\infty, & \text{otherwise} \end{cases}, \quad (11)$$

The path 4 length is the sum of the diameter of the planet pitch circle and  $l_{ri}$ ,

$$l_{si}(t) = l_{ri} + 2R_p. \quad (12)$$

This attenuation effect with regard to the path length can be characterized as window functions such as Hanning window or Gaussian window [11]. As demonstrated in Fig. 4(b), we apply the Gaussian window describing the time-varying transfer path effect,

$$\sigma(l) = F \exp\left(-\frac{l}{a}\right), \quad (13)$$

where  $l$  is the length of a transfer path,  $F$  represents for the strength factor and  $a$  is the attenuation factor.  $F$  is proportional to the input torque  $T_s$ , here we assume  $F = T_s/300$ . The larger  $a$  is, the longer impulses can propagate without a large energy loss. For simplicity, we set the  $\sigma_i(t) = \sigma[l_{ri}(t)] = \sigma_{ri}(t)$  and  $\eta = \exp(-\frac{2R_p}{a})$ . Fig. 4(a) shows

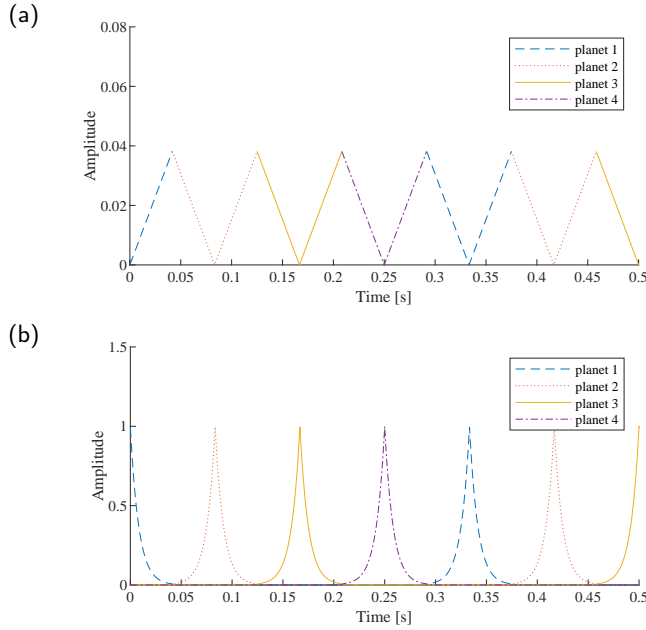


**Figure 4:** Transfer Path 1: (a) length function of time; (b) amplitude scaling effect.

that  $\sigma_i(t)$  shifts in time by  $(\epsilon_i + \Theta_i)/(2\pi f_c)$  relative to  $\sigma_1(t)$ :

$$\sigma_i(t) = \sigma_1(t - \frac{\epsilon_i + \Theta_i}{2\pi f_c}). \quad (14)$$

Because the transfer path effect function is an exponential function shifting along the time axis with a fixed interval, using the property of convolution and Delta function, it can be rewritten as the convolution of exponential function and Dirac comb function with the carrier rotation period  $1/f_c$ .

$$\sigma_{ri} = \sigma_i(t) = \sigma_0(t) * III \left[ f_c(t - \frac{\epsilon_i + \Theta_i}{2\pi f_c}) \right], \quad (15)$$

where convolution is denoted by  $*$ , and

$$\sigma_0(t) = \begin{cases} F \exp(-\frac{2\pi R_f f_c |t|}{a}), & \frac{-1}{2Mf_c} \leq t < \frac{1}{2Mf_c} \\ 0, & \text{otherwise.} \end{cases} \quad (16)$$

Given Eq. (12) and Eq. (13), we can deduce the proportional relationship between path 1 and path 4,

$$\sigma_{si}(t) = F \exp(-\frac{l_{ri} + 2R_p}{a}) = \exp(-\frac{2R_p}{a}) \cdot \sigma_i = \eta \cdot \sigma_0(t) * III \left[ f_c(t - \frac{\epsilon_i + \Theta_i}{2\pi f_c}) \right]. \quad (17)$$

where  $\eta = \exp(-\frac{2R_p}{a})$  is the scale difference between the planet-ring and planet-sun transfer path effects.

## 2.4. Natural frequency

In the above discussion, the gear meshing vibration is simply considered as Dirac impulses. In practice, every impact arising from different components will excite the machine natural frequency. The excited resonance affects the spectral structure globally: the amplitudes of the vibration frequencies around the natural frequency are reinforced and other amplitudes are attenuated. The resonance features a harmonic wave with the amplitude attenuating exponentially,

like the vibration of a spring-mass-damper,

$$\lambda(t) = \begin{cases} \exp(-t/\beta) \cdot \sin(2\pi f_n t), & t \geq 0 \\ 0, & t < 0 \end{cases}, \quad (18)$$

where  $\beta > 0$  is the structural damping coefficient,  $f_n$  is the natural frequency.

Every time a gear meshing vibration occurs, the machine's natural vibration is excited. Mathematically, this process is equivalent to the convolution of the impact function of the meshing vibration with the exponentially attenuated harmonic function of the natural vibration. Therefore, considering the effect of the natural vibration, the above signal model can be updated into

$$\tilde{x}(t) = \lambda(t) * \sum_{i=1}^M L_i \sigma_i(t) \left\{ \text{III} \left[ f_m \cdot \left( t - \frac{\epsilon_i + \Theta_i}{2\pi f_c} \right) \right] + \eta \text{III} \left[ f_m \cdot \left( t + \frac{\epsilon_i + \Theta_i}{2\pi f_s - 2\pi f_c} \right) + \frac{\varphi_i}{2\pi} \right] \right\}, \quad (19)$$

where  $*$  denotes convolution operator.

For machines with the same configuration, when the load distribution of the planet is uneven, the contact stiffness of the transfer path of each planet inside the planetary gearbox will decrease relative to the case of the uniform load distribution. As a result, The decrease of internal contact stiffness will lead to the decrease of natural frequency of the whole system. Therefore, the variation of the system's natural frequency can be used as a circumstantial evidence to diagnose the load distribution among planets.

If the planet pinhole distribute evenly on the carrier, the number of the planets bearing the input load varies as the applied load increases gradually. When the load starts at almost zero, only three planets or one pair of diagonal planets simultaneously engaging with sun and ring gear [16]. In this circumstance, load sharing factors  $L_i = 0$  for the unloaded planets. With the ascending input load, another pair of gears get involved. At the same time, the entire transmission system stiffen because more gears support the connection between the input and output. The natural frequency rises along with the system stiffness since the natural frequency equals the square root of stiffness over mass.

### 3. Spectral structure

In this section, we will derive the spectral structure of the above proposed signal model for the in-depth understanding of planetary gearbox vibration. Because natural vibration merely affects the spectral envelope shape, we can consider it separately later on. The gear meshing vibration (Eq. (4) and Eq. (5)) and transfer path effect arising from the carrier rotation  $\sigma_i(t)$  are periodic with periods  $1/f_m$  and  $1/f_c$ , respectively. According to Eq. (3) and  $f_r = 0$ ,  $f_m = Z_r \cdot f_c$ . Apply Fourier transform to the planet-ring vibration, yields

$$\begin{aligned} \mathcal{F} [\sigma_{ri}(t) \xi_{ri}(t)] &= \mathcal{F} \left\{ \sigma_0(t) * \text{III} \left[ f_c \cdot \left( t - \frac{\epsilon_i + \Theta_i}{2\pi f_c} \right) \right] \cdot A_{ri} \text{III} \left[ f_m \cdot \left( t - \frac{\epsilon_i + \Theta_i}{2\pi f_c} \right) \right] \right\} \\ &= A_{ri} \cdot \mathcal{F} [\sigma_0(t)] \cdot \mathcal{F} \left\{ \text{III} \left[ f_c \cdot \left( t - \frac{\epsilon_i + \Theta_i}{2\pi f_c} \right) \right] \right\} * \mathcal{F} \left\{ \text{III} \left[ f_m \cdot \left( t - \frac{\epsilon_i + \Theta_i}{2\pi f_c} \right) \right] \right\} \\ &= A_{ri} \cdot \hat{\sigma}_0(f) \cdot \frac{\text{III} \left( \frac{f}{f_c} \right) \exp \left[ -\frac{jf(\epsilon_i + \Theta_i)}{f_c} \right]}{\sqrt{2\pi} f_c} * \frac{\text{III} \left( \frac{f}{Z_r f_c} \right) \exp \left[ -\frac{jf(\epsilon_i + \Theta_i)}{f_c} \right]}{\sqrt{2\pi} Z_r f_c} \\ &= A_{ri} \cdot \frac{\hat{\sigma}_0(f)}{2\pi Z_r f_c^2} \cdot \sum_{m=-\infty}^{+\infty} \sum_{n=-\infty}^{+\infty} \delta [f - (mZ_r + n)f_c] \exp [-j(mZ_r + n)(\epsilon_i + \Theta_i)]. \end{aligned} \quad (20)$$

where  $\mathcal{F}\{\cdot\}$  denotes Fourier transform,  $\hat{\sigma}_0(f)$  is the Fourier spectrum of  $\sigma_0(t)$ ,  $\delta(t)$  denotes Dirac impulse. The convolution between two Dirac comb functions equals the summation of all shifted Dirac impulses. Similarly, the  $i$ -th

planet-sun gear vibration is:

$$\begin{aligned}
\mathcal{F} [\sigma_{si}(t)\xi_{si}(t)] &= \mathcal{F} \left\{ \eta \cdot \sigma_0(t) * \text{III} \left[ f_c(t - \frac{\epsilon_i + \Theta_i}{2\pi f_c}) \right] \cdot A_{si} \text{III} \left[ f_m \cdot (t + \frac{\epsilon_i + \Theta_i}{2\pi f_s - 2\pi f_c}) + \frac{\varphi_i}{2\pi} \right] \right\} \\
&= \eta \cdot A_{si} \cdot \mathcal{F} [\sigma_0(t)] \cdot \mathcal{F} \left\{ \text{III} \left[ f_c \cdot (t - \frac{\epsilon_i + \Theta_i}{2\pi f_c}) \right] \right\} * \mathcal{F} \left\{ \text{III} \left[ f_m \cdot (t + \frac{\epsilon_i + \Theta_i}{2\pi f_s - 2\pi f_c}) + \frac{\varphi_i}{2\pi} \right] \right\} \\
&= \eta \cdot A_{si} \cdot \hat{\sigma}_0(f) \cdot \frac{\text{III}(\frac{f}{f_c}) \exp \left[ \frac{-jf(\epsilon_i + \Theta_i)}{f_c} \right]}{\sqrt{2\pi} f_c} * \frac{\text{III}(\frac{f}{Z_r f_c}) \exp \left[ \frac{jf(\epsilon_i + \Theta_i)}{f_c - f_s} \right] \exp \left( \frac{\varphi_i f}{2\pi Z_r f_c} \right)}{\sqrt{2\pi} Z_r f_c} \\
&= \eta \cdot A_{si} \cdot \frac{\hat{\sigma}_0(f)}{2\pi Z_r f_c^2} \cdot \sum_{m=-\infty}^{+\infty} \sum_{n=-\infty}^{+\infty} \delta [f - (mZ_r + n)f_c] \exp [j(Z_s m - n)(\epsilon_i + \Theta_i)] \exp(jm\varphi_i),
\end{aligned} \tag{21}$$

where  $Z_s(f_c - f_s) = Z_r f_c = f_m$  is applied. Combine the above planet-ring and planet-sun vibration for all planets to obtain the Fourier transform of time-domain signal  $x(t)$  in Eq. (1):

$$\begin{aligned}
X(f) &= \sum_{i=1}^M L_i \cdot \{ \mathcal{F} [\sigma_{ri}(t)\xi_{ri}(t)] + \mathcal{F} [\sigma_{si}(t)\xi_{si}(t)] \} \\
&= \sum_{i=1}^M L_i \cdot \left\{ A_{ri} \cdot \frac{\hat{\sigma}_0(f)}{2\pi Z_r f_c^2} \cdot \sum_{m=-\infty}^{+\infty} \sum_{n=-\infty}^{+\infty} \delta [f - (mZ_r + n)f_c] \exp [-j(mZ_r + n)(\epsilon_i + \Theta_i)] \right. \\
&\quad \left. + \eta \cdot A_{si} \cdot \frac{\hat{\sigma}_0(f)}{2\pi Z_r f_c^2} \cdot \sum_{m=-\infty}^{+\infty} \sum_{n=-\infty}^{+\infty} \delta [f - (mZ_r + n)f_c] \exp [j(Z_s m - n)(\epsilon_i + \Theta_i)] \exp(jm\varphi_i) \right\} \\
&= \frac{\hat{\sigma}_0(f)}{2\pi Z_r f_c^2} \sum_{m=-\infty}^{+\infty} \sum_{n=-\infty}^{+\infty} \delta [f - (mZ_r + n)f_c] \left\{ \sum_{i=1}^M L_i \cdot A_{ri} \cdot \exp [-j(mZ_r + n)(\epsilon_i + \Theta_i)] \right. \\
&\quad \left. + \eta \cdot L_i \cdot A_{si} \cdot \exp(jm\varphi_i) \cdot \exp [j(mZ_r - n)(\epsilon_i + \Theta_i)] \right\}.
\end{aligned} \tag{22}$$

We assume the isotropy of planet and the amplitudes of  $i$ -th planet gear meshing impacts  $A_{ri}$  and  $A_{si}$  remain the same for every planet, that is  $A_{ri} = A_{r1}$ ,  $A_{si} = A_{s1}$ . When all planets locate at the nominal positions ( $\epsilon_i = 0$ ), each planet bears the same torque ( $L_i = L_1$ ), The Fourier transform  $X(f)$  in the ‘perfect’ case is

$$\begin{aligned}
X(f) &= \frac{L_1 \cdot \hat{\sigma}_0(f)}{2\pi Z_r f_c^2} \sum_{m=-\infty}^{+\infty} \sum_{n=-\infty}^{+\infty} \delta [f - (mZ_r + n)f_c] \left\{ \sum_{i=1}^M A_{ri} \exp [-j(mZ_r + n)\Theta_i] \right. \\
&\quad \left. + \eta A_{s1} \exp(jm\varphi_i) \exp [j(mZ_r - n)\Theta_i] \right\},
\end{aligned} \tag{23}$$

where

$$\sum_{i=1}^M \exp[-j(mZ_r + n)\Theta_i] = \sum_{i=1}^M \exp[-j(mZ_r + n)\frac{2\pi(i-1)}{M}] = \begin{cases} M, & \frac{mZ_r + n}{M} \in \mathbb{N} \\ 0, & \frac{mZ_r + n}{M} \notin \mathbb{N} \end{cases}, \tag{24}$$

$$\sum_{i=1}^M \exp[j(mZ_s - n)\Theta_i] = \sum_{i=1}^M \exp[j(mZ_s - n)\frac{2\pi(i-1)}{M}] = \begin{cases} M, & \frac{mZ_s - n}{M} \in \mathbb{N} \\ 0, & \frac{mZ_s - n}{M} \notin \mathbb{N} \end{cases}. \tag{25}$$

According to the above Eq. (24) and Eq. (25), when  $(mZ_r + n)$  or  $(mZ_s - n)$  is the multiple of planet number  $M$ , the corresponding Fourier coefficient is nonzero. The carrier harmonics only peak at the multiple of planet number

**Table 1**

Parameters of simulated signals: (a) configuration parameters; (b) other parameters.

| (a) | Ring gear teeth $Z_r$    | Planet pitch radius $R_p$ | Ring gear pitch radius $R_r$ | Sun gear pitch radius $R_s$  | Phase difference $\varphi$ |
|-----|--------------------------|---------------------------|------------------------------|------------------------------|----------------------------|
|     | 61                       | 15.75 mm                  | 48.60 mm                     | 16.20 mm                     | $8.727 \times 10^{-4}$ rad |
| (b) | Sampling frequency $F_s$ | Duration                  | Carrier frequency $f_c$      | Input torque $T_s$ (default) | Strength factor $F$        |
|     | $10^4$ Hz                | 10 s                      | 3 Hz                         | 300 N m                      | 1                          |
|     |                          |                           |                              |                              | $7.634 \times 10^{-3}$     |
|     |                          |                           |                              |                              | $2.975 \times 10^7$ N/m    |

$M$  when planet distributes evenly. Interestingly, all planet distributes evenly ( $\epsilon_i = 0$ ) can only be achieved when the condition  $(Z_r + Z_s)/M \in \mathbb{N}$  is guaranteed (explanations see Appendix). Therefore,  $(mZ_r + n)/M$  and  $(mZ_s - n)/M$  will be integers at one time.

When  $\epsilon_i \neq 0$ , all carrier harmonic  $(mZ_r + n)$  and  $(mZ_s - n)$  will appear with their amplitude arising from planet-ring meshing ( $\sum_{i=1}^M L_i \exp[-j(mZ_r + n)(\epsilon_i + \Theta_i)]$ ) and planet-sun meshing ( $\sum_{i=1}^M L_i \exp[-j(mZ_s - n)(\epsilon_i + \Theta_i)]$ ), respectively. For example, the second planet carries all load (the  $L_2 = 1$  and  $L_i = 0, i \neq 2$ ), the  $(mZ_r + n)$  order harmonic manifests itself with the amplitude of  $\sum_{i=1}^M L_i \exp[-j(mZ_r + n)(\epsilon_i + \Theta_i)]$ , which is nonzero. The amplitudes of the planet number multiples of carrier harmonics scale down to  $\exp[j(mZ_r + n)\epsilon_i]$  and  $\exp[j(mZ_s - n)\epsilon_i]$ , respectively.

Natural vibration further scales the amplitude of spectral components. Apply the convolution theorem to the signal model considering natural vibration (Eq. (19)), the final version of spectrum:

$$\tilde{X}(f) = \mathcal{F}[\lambda(t) * x(t)] = \mathcal{F}[\lambda(t)] \cdot \mathcal{F}[x(t)] = \hat{\lambda}(f) \cdot \tilde{X}(f) \quad (26)$$

where  $\hat{\lambda}(f)$  is the Fourier transform of  $\lambda(t)$ :

$$\hat{\lambda}(f) = \frac{\sqrt{2\pi}\beta^2 f_n}{-4\pi^2\beta^2 f^2 + 4\pi^2\beta^2 f_n^2 + 1 - j4\pi\beta f} \quad (27)$$

## 4. Discussion on model factors

We use MATLAB® to simulate the proposed signal model. To validate the generality of the propose model, we take different planet pinhole position errors, planet numbers and input torques into account. The simulation parameters are listed in Table 1.

In general, if the planet locates the nominal position, only the planet number multiples of carrier harmonics appear (give more specific results in figures), which accords with the Eq. (24) and Eq. (25). When the planet center deviates from the nominal position, other carrier orders emerges. Differing from the conclusion in [11], the dominant planet number multiple peaks do not necessarily shrink too, because we also consider the phase modulation induced by the pinhole position errors.

The amplitude envelope sharpe can also evidence the existence of planet position shifts. Because the support stiffness weakens, the resonance frequency of the entire system shift towards the y-axis. Fig. 5 explain the mechanism of shifted natural frequency – the resonance frequency shift from 230 carrier orders to 170 carrier orders. With the limited measurement conditions about natural frequency in industrial applications, the above natural frequency shift can only be validated qualitatively. The signal model in Eq. (19) indicates the natural frequency affects the spectral envelope shape. As the load increases, the envelope peak shifting to a higher frequency signifies the unequal load sharing among planets.

### 4.1. Different planet numbers

When at least one central members can float along the radial direction, the floating motion in three planet gearbox can offset the influence of uneven load distribution arising from limited pinhole position errors. The condition of floating central members can be satisfied commonly, because the manufacturers deliberately design separable sun gears

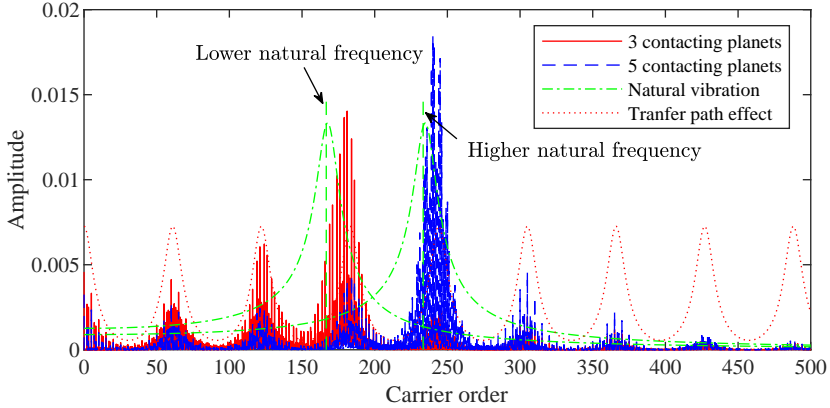


**Figure 5:** Spectral summit cluster shifts towards a lower frequency due to the uneven load distribution of planets.

and flexible couplings. When tangential errors in planet pinhole occur, the time shifts to the transfer path effect still make the impulsive intervals uniform between adjacent planets. Fig 6(b) present a quasi phase modulation – if we regard all planets as one – in time domain. The corresponding spectrum also manifests the non planet number ( $M = 3$ ) peaks. In the baseline case where these pinhole errors are absent, the carrier orders merely appear at the multiples of three.

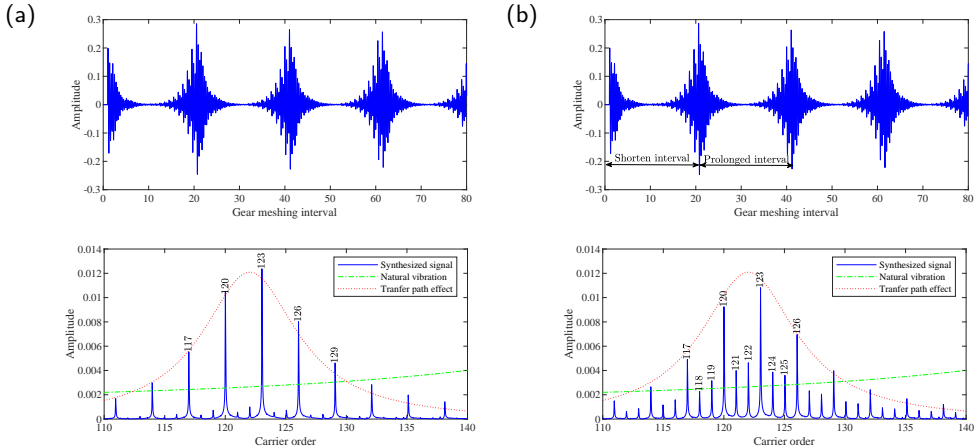


**Figure 6:** Simulated signals of planetary boxes of 3 planets: (a) normal case; (b)  $0.5^\circ$  angular position error on second planet pinhole.

In cases where planet number  $M \geq 4$ , floating members in planetary gearboxes cannot neutralize all the effects on load sharing conditions caused by planet pinhole position errors. The time domain signals in Fig. 7(b) ( $M = 4$ ) demonstrates the pinhole errors modulates the timing and strength of each planet impulse at the same time. Shown in the Fourier spectra of fault cases, the quasi amplitude and frequency modulation gives rise to the extra sidebands emerge at the non  $M$  multiples. While carrier orders only peak with the intervals of planet number in Fig. 7(a) ( $M = 4$ ).

#### 4.2. Effects of input torque

As explained in the Section 2.3, the input torque affects the impulsive strengths of planets contacting with sun and ring gears, so as to scale the whole signal amplitudes. Fig. 8 shows that the larger input torque is applied, the higher signal amplitude in both time and frequency domains.

The input torque also affects the numbers of contacting planets. As the input torque increases from a lower value,

### Unequal planet load sharing

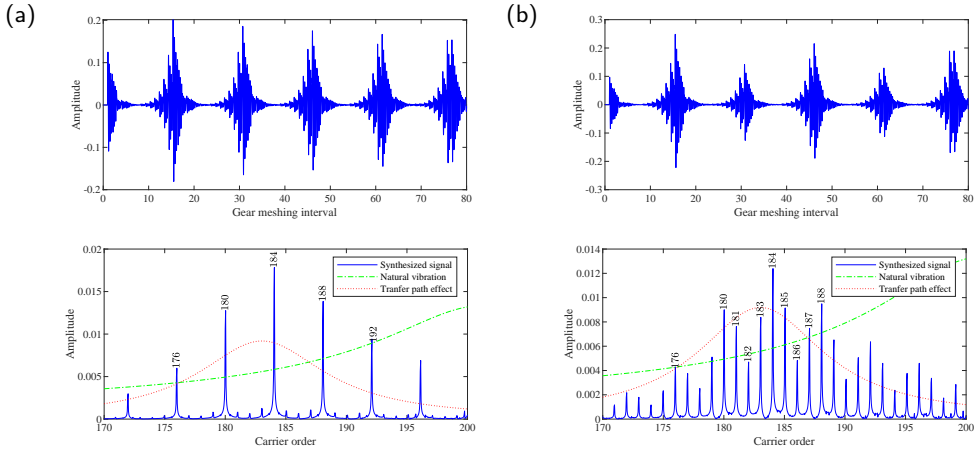


**Figure 7:** Simulated signals of planetary boxes of 4 planets: (a) normal case; (b)  $0.5^\circ$  angular position error on second planet pinhole.

more planets get involved in bearing load gradually. Thus, the natural frequency of the system rises. Fig. 9 presents the natural frequency shift in spectrum. In addition, the larger input torque can improve load sharing conditions to be more uniform. Extra non M multiples shrinks relatively to the dominant M multiples.

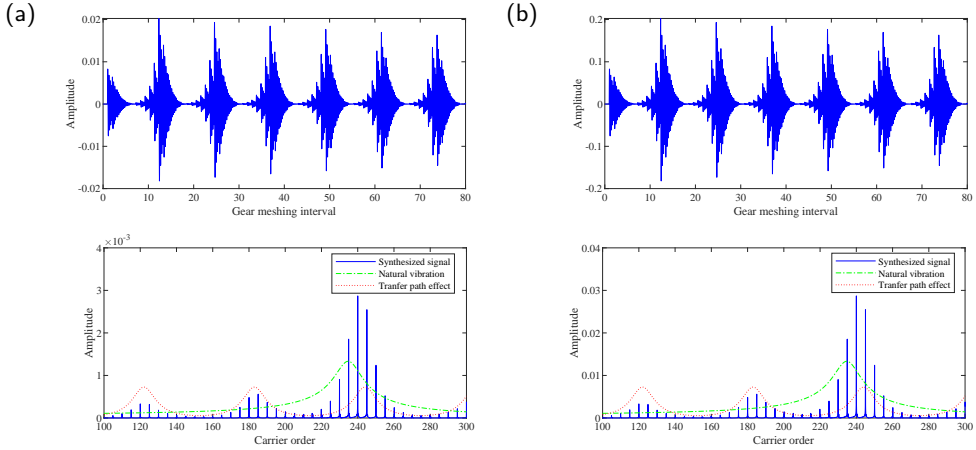


**Figure 8:** Simulated signals of normal planetary boxes with different input torques: (a)  $T_s = 30 \text{ N m}$ ; (b)  $T_s = 300 \text{ N m}$ .

#### 4.3. Severity levels of pinhole error

The severity of pinhole error mainly influences the signal spectra in two stages. At the beginning the planetary gearbox is free of pinhole errors. All planets bear the load evenly with the same strength as shown in time domain of Fig. 10(a), and peaks only exist at the multiples of planet number ( $M = 6$ ). When a slight error ( $0.1^\circ$  on the fourth planet pinhole) occurs, Fig. 10(b) demonstrates the non M multiples of carrier orders emerge in spectrum. At the first stage, an increasing error level ( $1^\circ$ ) leads to the amplified the components of non M multiples clustering around the dominant peaks, as presented in Fig. 10(c). At the second stage, if we continually enlarges the error to  $2.1^\circ$ , a pair of planets will separate from contact and the location of envelope summit along with the system natural frequency will decrease to a lower range. Fig. 10(d) illustrates this phenomenon.

## 5. Experimental validation

We implemented experiments to substantiate the proposed signal model and the above theoretical derivation.

## Unequal planet load sharing

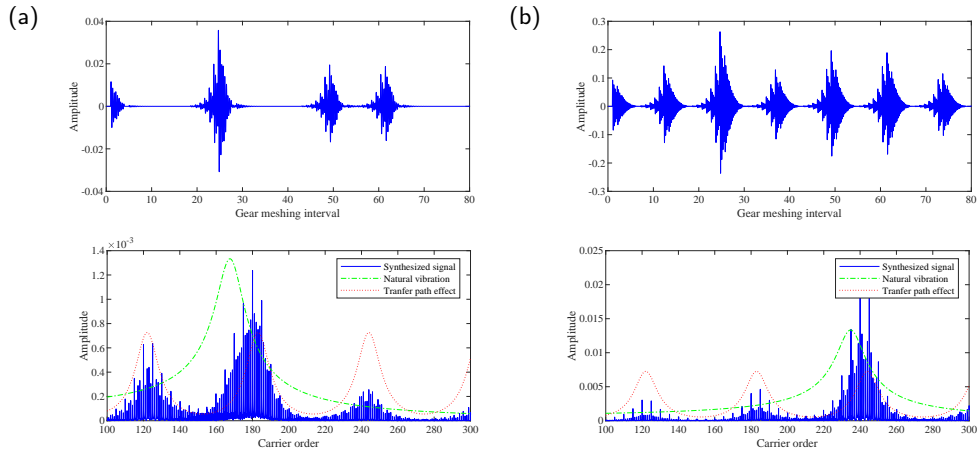


**Figure 9:** Simulated signals of faulty planetary boxes with  $0.4^\circ$  error in the third planet pinhole and different input torques: (a)  $T_s = 30 \text{ N m}$ ; (b)  $T_s = 300 \text{ N m}$ .

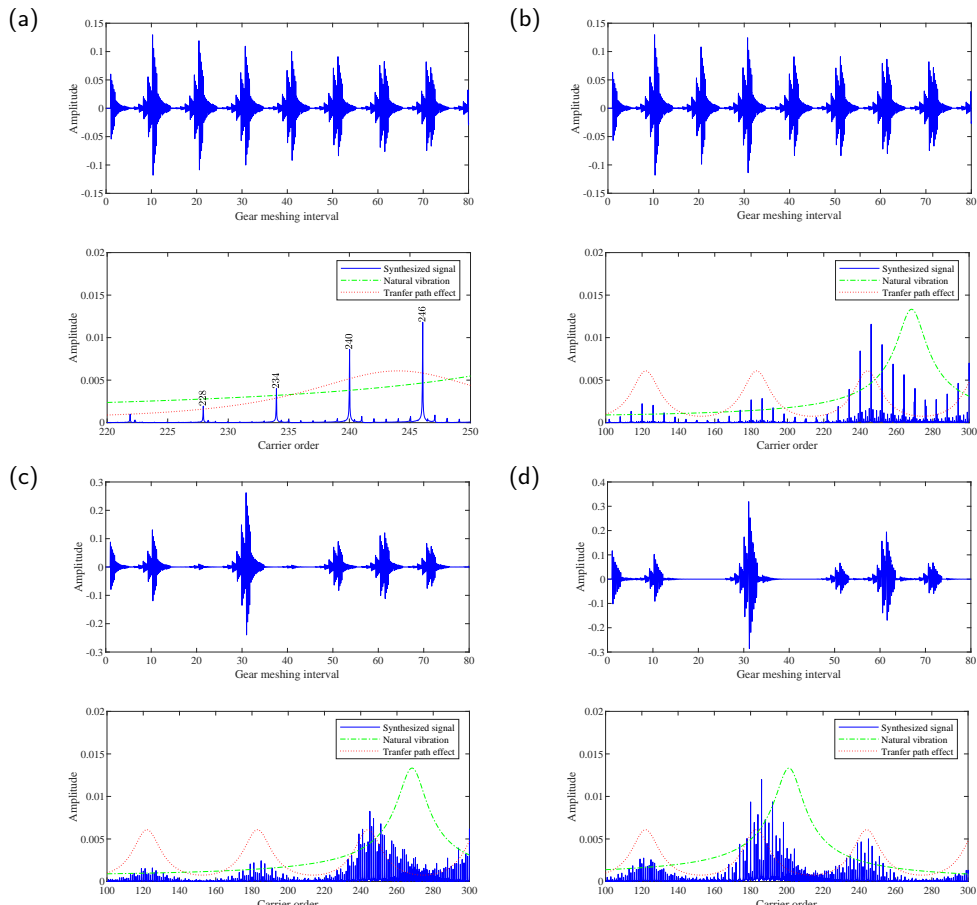


**Figure 10:** Simulated signals of planetary boxes with errors on the fourth planet in various severity levels: (a) normal; (b)  $0.1^\circ$ ; (c)  $1^\circ$ ; (d)  $2.1^\circ$ .

**Table 2**

Rated parameters of planetary gearbox.

| Power (kW) | Speed (rpm) | Speed ratio |
|------------|-------------|-------------|
| 8          | 507         | 4           |

**Table 3**

Confiurion parameters of planetary gearbox.

| Gear            | Sun gear | Planet (number) | Ring gear |
|-----------------|----------|-----------------|-----------|
| Number of teeth | 36       | 35 (3)          | 108       |

## 5.1. Experimental settings

We set up a test rig consisting of a motor, a planetary gearbox, an encoder, a torque transducer and a generator as load, as shown in Fig. 11. Besides a normal planetary gearbox with four planets as baseline, we designed a fault case where one planet pinhole ahead of the nominal position by  $0.1^\circ$ , demonstrated in Fig. 12. The rated parameters and configuration parameters of the planetary gearbox are listed in Table 2 and Table 3, respectively. The sampling frequency of the acquisition system is 20480 Hz, and the duration is 60 s. The rotating frequency of sun gear is 8.45 Hz (507 rpm). 30 N m load is applied. The gear meshing frequency is  $f_m = 228.15$  Hz and carrier frequency is  $f_c = 2.1125$  Hz.

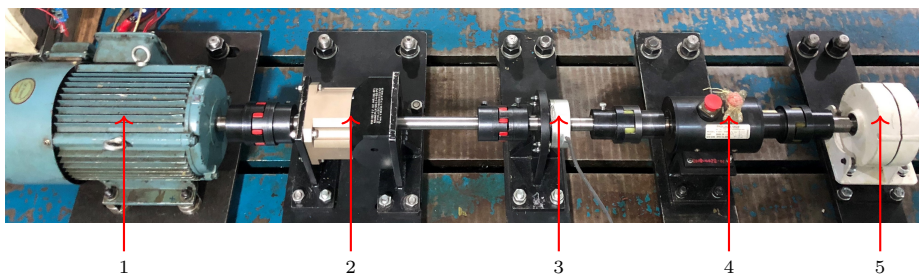


**Figure 11:** Planetary gearbox test rig: 1. induction motor; 2. planetary gearbox; 3. rotary encoder; 4. torque transducer and 5. generator.



**Figure 12:** Planetary gearbox with a pinhole position error.

## 5.2. Experimental data analysis

Fig. 13 overviews the spectra of normal and fault cases. Generally, the natural vibration and transfer path effect jointly shape the envelopes of the normal and fault spectra. By contrast, the envelope summit of normal spectrum

locates at the higher frequency range than the fault case since the natural frequency of normal case is higher. This indicates that the pinhole position error can cause planets to disconnect with sun or ring gears, verifying the natural frequency shift described in Section 2.4.

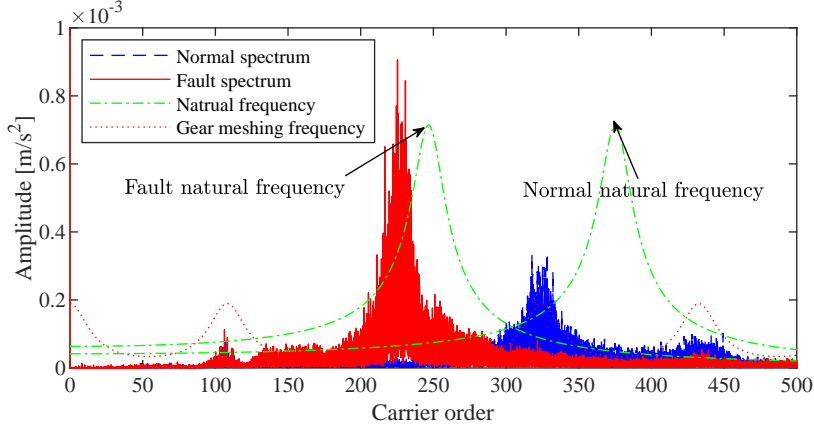


**Figure 13:** Spectrum overview of experimental data.

The signal in fault case displays more irregular impulses within one carrier rotation period, demonstrated in Fig. 14(b). While the impulsive amplitudes and intervals are more evenly distributed in the normal case (Fig. 14(a)). By comparison between frequency domains, non M multiples of carrier order peaks clearly in the fault case, evidencing the non-uniform load distribution among planets. The unconspicuous noise components are attributed to the inevitable errors during manufacturing and assembling.

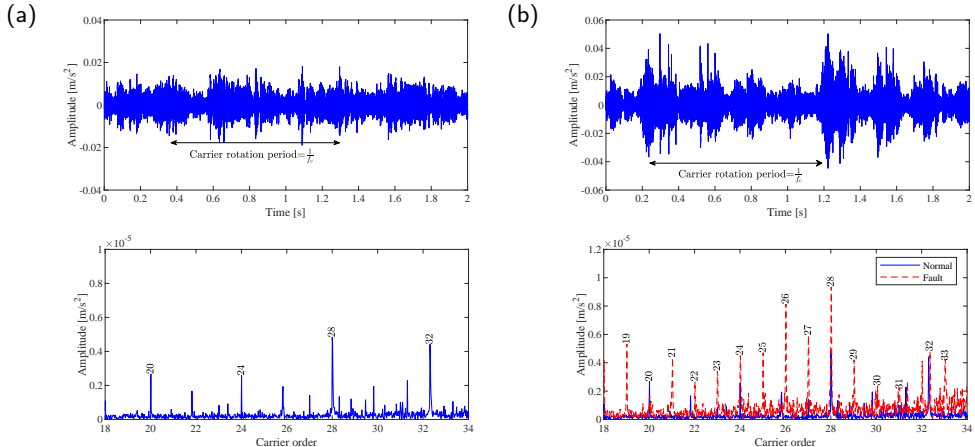


**Figure 14:** Experimental data analysis in time and frequency domains: (a) normal case; (b) fault case.

## 6. Conclusions

We established a vibration signal model of planetary gearboxes and derived the corresponding Fourier spectrum, considering the effect of transfer path, gear meshing vibration, natural vibration, amount of contacting planets and load sharing among planets. Only planet number multiples of carrier rotating frequency appear in the Fourier spectrum of the normal case, while the spectrum of unequal load sharing signal additionally presents non planet number multiples of carrier rotating frequency. The pinhole position error severity and the input torque jointly affect the load sharing conditions, the number of contacting planets and the system natural frequency. With the increasing pinhole error

severity or the decreasing applied input torque, fewer planets bear loads, the stiffness of the whole system decreases, the natural frequency shifts towards a lower range and the load sharing conditions deteriorate. Thus, the additional carrier orders and the shifted natural frequency in the spectrum can evidence the unequal load sharing among planets for diagnostic purposes. In the future, we will investigate the modeling of unequal load sharing among planets with the existence of gear and bearing faults.

## Appendix

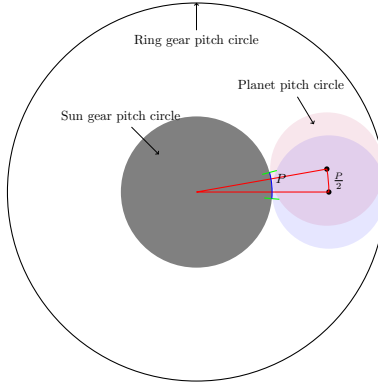


**Figure 15:** The minimum angle between two adjacent planet possible positions.

As shown in Fig. 15. The pitch circle of planet gear rolls along the pitch circle of sun gear. When sun gear and ring gear are both fixed, the planet can only assembled at finite discrete angular positions. The minimum angular between two adjacent positions can be calculated as follows. Imagine the sun gear ‘rotates’ an entire tooth, and a planet rotates a distance along with the pinhole circle on the carrier. The transmission ratio between carrier and sun gear is

$$\text{Transmission ratio} = \frac{Z_s}{Z_s + Z_r} \quad (28)$$

the angle the sun gear rotates is:  $\frac{P}{R_s}$ , where  $P$  is the tooth spacing (base pitch). So the distance the pinhole center rotates is

$$(R_s + R_p) \cdot \frac{P}{R_s} \cdot \frac{Z_s}{Z_s + Z_r} = \frac{R_s + R_p}{R_s + R_r} \cdot P = \frac{R_s + R_p}{R_s + R_s + 2R_p} \cdot P = \frac{P}{2} \quad (29)$$

Thus, the angle the planet-carrier rotates is

$$\lambda = \frac{P}{2} \cdot \frac{1}{R_p + R_s} = \frac{P}{R_r + R_s} \quad (30)$$

According to the definition of module of gear  $m = \frac{D}{Z} = \frac{P}{\pi}$ , the Eq. (30) can be rewritten as:

$$\lambda = \frac{P \cdot 2}{D_r + D_s} = \frac{2\pi m}{m \cdot (Z_r + Z_s)} = \frac{2\pi}{Z_r + Z_s}, \quad (31)$$

The planets can only locate finite angular positions with minimum space . When planets locate uniformly at angular positions  $\frac{2\pi(i-1)}{M}$ , the  $Z_r + Z_s$  must be an integer multiple of planet number  $M$ .

## References

- [1] Z. P. Feng, M. J. Zuo, Vibration signal models for fault diagnosis of planetary gearboxes, *Journal of Sound and Vibration* 331 (22) (2012) 4919–4939.
- [2] D. Zhao, T. Wang, F. Chu, Deep convolutional neural network based planet bearing fault classification, *Computers in Industry* 107 (2019) 59–66.
- [3] A. Singh, Load sharing behavior in epicyclic gears: physical explanation and generalized formulation, *Mechanism and machine theory* 45 (3) (2010) 511–530.
- [4] D. L. Seager, Load sharing among planet gears, *SAE Transactions* (1970) 651–656.
- [5] A. Bodas, A. Kahraman, Influence of carrier and gear manufacturing errors on the static load sharing behavior of planetary gear sets, *Jsm International Journal Series C-Mechanical Systems Machine Elements And Manufacturing* 47 (3) (2004) 908–915.
- [6] H. Ligata, A. Kahraman, A. Singh, An experimental study of the influence of manufacturing errors on the planetary gear stresses and planet load sharing, *Journal of Mechanical Design* 130 (4) (2008) 041701.
- [7] A. Kahraman, Load sharing characteristics of planetary transmissions, *Mechanism and Machine Theory* 29 (8) (1994) 1151–1165.
- [8] A. Singh, Application of a system level model to study the planetary load sharing behavior, *Journal of Mechanical Design* 127 (3) (2005) 469–476.
- [9] P. McFadden, J. Smith, An explanation for the asymmetry of the modulation sidebands about the tooth meshing frequency in epicyclic gear vibration, *Proceedings of the Institution of Mechanical Engineers, Part C: Journal of Mechanical Engineering Science* 199 (1) (1985) 65–70.
- [10] M. Inalpolat, A. Kahraman, A theoretical and experimental investigation of modulation sidebands of planetary gear sets, *Journal of Sound and Vibration* 323 (3) (2009) 677–696.
- [11] W. D. Mark, J. A. Hines, Stationary transducer response to planetary-gear vibration excitation with non-uniform planet loading, *Mechanical Systems and Signal Processing* 23 (4) (2009) 1366–1381.
- [12] Y. G. Lei, Z. Y. Liu, J. Lin, F. B. Lu, Phenomenological models of vibration signals for condition monitoring and fault diagnosis of epicyclic gearboxes, *Journal of Sound and Vibration* 369 (2016) 266–281.
- [13] P. Velex, L. Flamand, Dynamic response of planetary trains to mesh parametric excitations, *Journal of mechanical design* 118 (1) (1996) 7–14.
- [14] G. D. Acar, B. F. Feeny, Approximate floquet analysis of parametrically excited multi-degree-of-freedom systems with application to wind turbines, *Journal of vibration and acoustics* 141 (1).
- [15] R. G. Parker, J. Lin, Mesh phasing relationships in planetary and epicyclic gears, *Journal of Mechanical Design* 126 (2) (2004) 365–370.
- [16] H. Ligata, A. Kahraman, A. Singh, A closed-form planet load sharing formulation for planetary gear sets using a translational analogy, *Journal of mechanical design* 131 (2).